Nuclear Instruments and Methods in Physics Research A 593 (2008) 530–538

Contents lists available at ScienceDirect

Nuclear Instruments and Methods in Physics Research A

journal homepage: www.elsevier.com/locate/nima

Effects of the temperature dependence of the signals from lead tungstate crystals

N. Akchurin [a], M. Alwarawrah [a], A. Cardini [b], G. Ciapetti [c], R. Ferrari [d], S. Franchino [d], M. Fraternali [d], G. Gaudio [d], J. Hauptman [e], F. Lacava [c], L. La Rotonda [f], M. Livan [d], M. Mancino [d], E. Meoni [f], H. Paar [g], D. Pinci [c], A. Policicchio [f], S. Popescu [a], G. Susinno [f], Y. Roh [a], W. Vandelli [h], T. Venturelli [f], C. Voena [c], I. Volobouev [a], R. Wigmans [a,*]

[a] Texas Tech University, Lubbock, TX, USA
[b] Dipartimento di Fisica, Università di Cagliari and INFN Sezione di Cagliari, Italy
[c] Dipartimento di Fisica, Università di Roma "La Sapienza" and INFN Sezione di Roma, Italy
[d] Dipartimento di Fisica Nucleare e Teorica, Università di Pavia and INFN Sezione di Pavia, Italy
[e] Iowa State University, Ames, IA, USA
[f] Dipartimento di Fisica, Università della Calabria and INFN Cosenza, Italy
[g] University of California at San Diego, La Jolla, CA, USA
[h] CERN, Genève, Switzerland

ARTICLE INFO

Article history:
Received 31 March 2008
Received in revised form
7 May 2008
Accepted 13 May 2008
Available online 23 May 2008

Keywords:
Lead tungstate crystals
Cherenkov light
Decay time
Temperature effects

ABSTRACT

The signals from lead tungstate crystals are studied as a function of temperature. Over the range from 13 to 45 °C, the total light output decreases by about a factor of two. This effect only concerns the scintillation component, so that the relative contribution of Cherenkov light to the signals increases with the same factor. The decay time of the scintillation component is observed to decrease as well.

1. Introduction

In a recent paper, we demonstrated that a significant fraction of the signals from scintillating lead tungstate ($PbWO_4$) crystals is due to Cherenkov radiation [1]. This was concluded from the measurements of the time structure of the signals and the non-isotropic nature of the light generated by high-energy electrons and muons traversing a $PbWO_4$ crystal. In the crystal used for these studies, Cherenkov light contributed up to 15% of the signals measured by a photomultiplier tube (PMT).

It is well known that $PbWO_4$ crystals, which are the detectors of choice in several modern large-scale experiments in high-energy and medium-energy physics [2], are very delicate. Mechanically, they are very fragile and their scintillation properties are significantly affected by small changes in temperature [3] and by small radiation doses [4]. In this paper, we examine the temperature dependence of the scintillation properties, including the total light output, the contribution of Cherenkov light to the signals and the decay time of the signals in a temperature range of about 30° around room temperature. We want to emphasize that all results presented in this paper were obtained by studying one particular crystal,[1] and are therefore not necessarily representative for all crystals made of this material. However, while the detailed numbers may differ, we believe that the overall trends reported in this study are a general feature of this type of crystal. We base this on the fact that these trends have also been observed in a matrix made of 19 identical $PbWO_4$ crystals [5]. In Section 2, the detectors and the experimental setup in which they were tested are described, as well as the calibration and data analysis methods that were used. Experimental results are presented in Section 3, and conclusions drawn in Section 4.

* Corresponding author. Fax: +1 806 742 1182.
E-mail address: wigmans@ttu.edu (R. Wigmans).

[1] The crystals used for these studies were provided by the ALICE Collaboration, who use $PbWO_4$ for their PHOS calorimeter.

0168-9002/$ - see front matter © 2008 Elsevier B.V. All rights reserved.
doi:10.1016/j.nima.2008.05.025

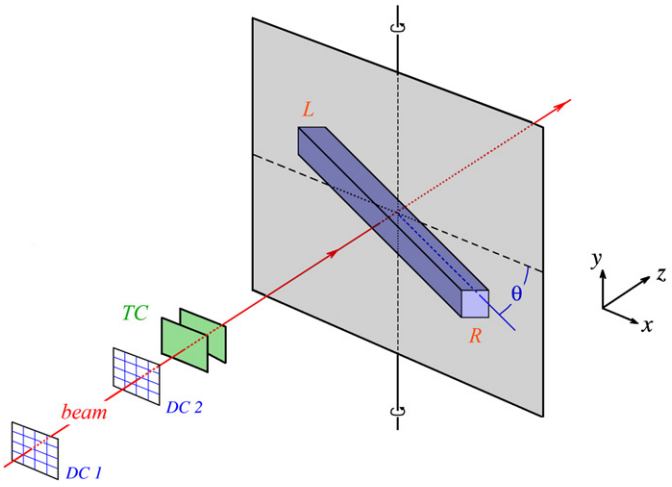

Fig. 1. Experimental setup in which the beam tests were performed.

2. Equipment and measurements

2.1. Detectors and beam line

The measurements described in this paper were performed in the H4 beam line of the Super Proton Synchrotron at CERN. Our detector was a $PbWO_4$ crystal with a length of 18 cm and a cross-section of $2.2 \times 2.2\,cm^2$. The transverse dimension, relevant for our measurements, corresponds to 2.5 radiation lengths. All six sides of this crystal were polished, and for the measurements described in this paper, it was loosely wrapped in aluminized mylar. The light produced by particles traversing this crystal was read out by two PMTs,[2] *L* and *R*, located at opposite ends. In order to reduce the light trapping effects of the large refractive index of $PbWO_4$, the PMTs were coupled to the crystal by means of silicone "cookies" ($n_c = 1.403$).

This crystal was mounted on a platform that could rotate around a vertical axis. The crystal was oriented in the horizontal plane and the rotation axis went through its geometrical center. The particle beam was also steered through this center, as illustrated in Fig. 1. The angle θ, which is frequently used in the following, represents the angle between the crystal axis and a plane perpendicular to the beam line. The angle increases when the crystal is rotated such that the crystal axis *L*–*R* approaches the direction of the traveling beam particles. The crystal orientation shown in Fig. 1 corresponds thus to $\theta < 0$.

Two small scintillation counters provided the signals that were used to trigger the data acquisition system. These trigger counters (TC) were 2.5 mm thick, and the area of overlap was $6 \times 6\,cm^2$. A coincidence between the logic signals from these counters provided the trigger. The trajectories of individual beam particles could be reconstructed with the information provided by two small drift chambers (DC1, DC2) which were installed upstream of the TC. This system made it possible to determine the location of the impact point of the beam particles at the calorimeter with a precision of typically ~0.2 mm.

2.2. Temperature control

The temperature of the crystal was controlled by means of a thermoelectric system, based on the Peltier effect. A thermal conductive paste was used to increase the coupling efficiency between the crystal and the thermoelectric plate. With a computer-controlled system, it was possible to achieve a reasonably stable operation between 13 and 43 °C for this setup. One thermistor measured the temperature on top of the crystal, while another monitored the temperature of the thermoelectric plate. A programmable feedback logic circuit controlled the output of the power supply driving the thermoelectric plate. The net heating or cooling effect was proportional to the electric current and the Peltier coefficient.

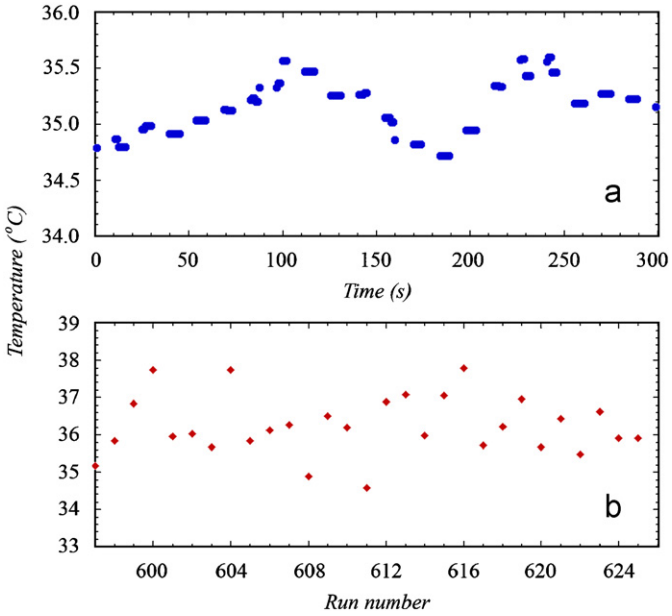

Fig. 2. Typical temperature stability of the crystal during a 5-min run (a) and during an entire angular scan of several hours (b).

Fig. 2 shows typical data of the temperature stability of this setup. These data, taken at a nominal crystal temperature of 35 °C (and room temperature of 20 °C), indicate that the temperature variations during a 100 000 event run lasting 5 min. were limited to ±0.3 °C, and that the variations that occurred during an entire angular scan (3–5 h) were typically limited to ±1 °C around the average value.

2.3. Data acquisition

Measurement of the time structure of the crystal signals formed a very important part of the tests described here. In order to limit distortion of this structure as much as possible, we used special, 15 mm thick cables to transport the detector signals to the counting room. Such cables were also used for the signals from the TC, and these were routed such as to minimize delays in the DAQ system.[3]

The crystal signals were sent into a unity-gain Linear Fan-out unit, output signals of which were used to measure the time structure and the total charge. The time structure was measured with a sampling oscilloscope,[4] which measured the amplitude of the signals at a rate of 2.5 GHz. The $PbWO_4$ signals were measured over a time interval of 112 ns, during which 282 data points were collected.

The quality of the information obtained in this way is illustrated in Fig. 3, which shows the average time structure of the signals from PMT *L* generated by 50 GeV electrons traversing the crystal at $\theta = 30°$.

[2] Hamamatsu R5900U, 10-stage, bialkali photocathode, borosilicate window.

[3] We measured the signal speed to be 0.78*c* in these cables.

[4] Tektronix TDS7254B, four channels, analog bandwidth 2.5 GHz, sampling frequency up to 20 Gsample/s in 1 channel.

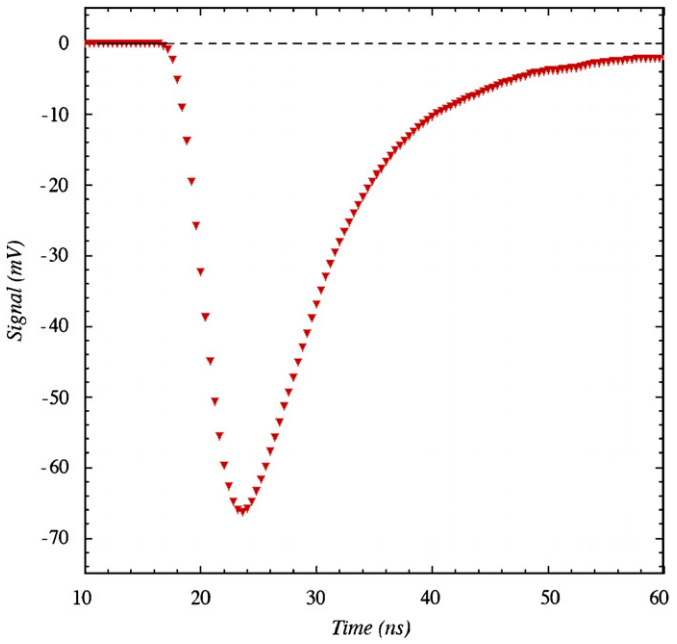

Fig. 3. Average time structure of the signals from PMT L measured for 50 GeV electrons traversing the $PbWO_4$ crystal at $\theta = 30^\circ$.

The charge measurements were performed with 12-bit Caen ADCs (V792). These had a sensitivity of 100 fC/count and a conversion time of 5.7 μs. The ADC gate width was 100 ns, and the calorimeter signals arrived ~20 ns after the start of the gate.

The data acquisition system used VME electronics. A single VME crate hosted all the needed readout and control boards. The trigger logic was implemented through NIM modules and the signals were sent to a VME I/O register, which also collected the spill and the global busy information. The VME crate was linked to a Linux based computer through an SBS 620[5] optical VME–PCI interface that allowed memory mapping of the VME resources via an open source driver.[6] The computer was equipped with a 2 GHz Pentium-4 CPU, 1 GB of RAM, and was running a CERN SLC 4.3 operating system.[7]

The data acquisition was based on a single-event polling mechanism and performed by a pair of independent programs that communicated through a first-in-first-out buffer, built on top of a 32 MB shared memory. Only exclusive accesses were allowed and concurrent requests were synchronized with semaphores. The chosen scheme optimized the CPU utilization and increased the data taking efficiency by exploiting the bunch structure of the SPS, where beam particles were provided to our experiment during a spill of 4.8 s, out of a total cycle time of 16.8 s. During the spill, the readout program collected data from the VME modules and stored them into the shared memory, with small access times. During the remainder of the SPS cycle, a recorder program dumped the events to the disk. Moreover, the buffer presence allowed low-priority monitoring programs to run (off-spill) in spy mode. With this scheme, we were able to reach a data acquisition rate as high as 2 kHz, limited by the FADC readout time. The typical event size was ~1 kB. All detector signals were monitored online.

[5] http://www.gefanucembedded.com/products/457
[6] http://www.awa.tohoku.ac.jp/~sanshiro/kinoko-e/vmedrv/
[7] http://linux.web.cern.ch/linux/scientific4/

2.4. Experimental data and analysis methods

The $PbWO_4$ crystal was exposed to a 50 GeV electron beam. The angle θ between the crystal axis and the plane perpendicular to the beam line was varied from -60° to 60°, in steps of 5°. At each angle, 100 000 events were collected. In addition, 10 000 randomly triggered events provided pedestal information. This measurement cycle was carried out for four different temperatures: 13, 25, 35 and 45 °C. A smaller cycle of runs, involving angles $\theta = 0$, $\pm 25^\circ$, $\pm 30^\circ$ and $\pm 35^\circ$, was carried out for intermediate temperatures: 15, 20, 30 and 40 °C. Also at these temperatures, 100 000 events were collected for each run, plus 10 000 pedestal events (random triggers). Fig. 4 shows the order in which these scans were performed.

Off-line, the beam chamber information could be used to select events that entered the crystal in a small region located around its geometric center. The beam contained a very small fraction of muons, which were eliminated with help of the downstream muon counter.

Fig. 5 shows a typical ADC signal distribution, measured by one of the two PMTs connected to the crystal. A ~1% beam contamination of pions left a MIP signal in the crystal (highlighted in Fig. 5), which was well separated from the signals produced by

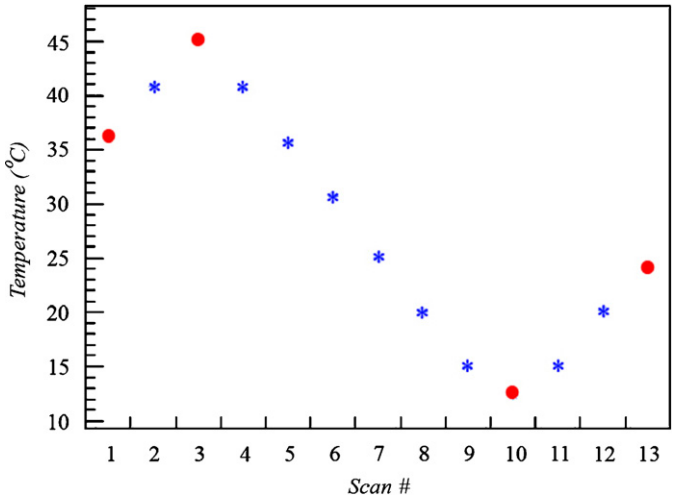

Fig. 4. The order in which the different angular scans were performed, i.e., the temperature cycle of the crystal. Points at which a full complement of angular measurements was performed are indicated by full circles.

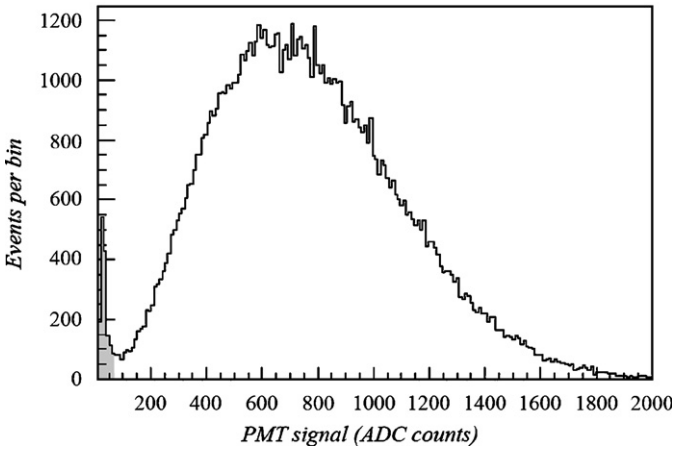

Fig. 5. Signal distribution for 50 GeV electrons showering in a $2.5X_0$ thick $PbWO_4$ crystal, measured by one of the PMTs. The highlighted part of the spectrum is the result of the pion contamination in the beam.

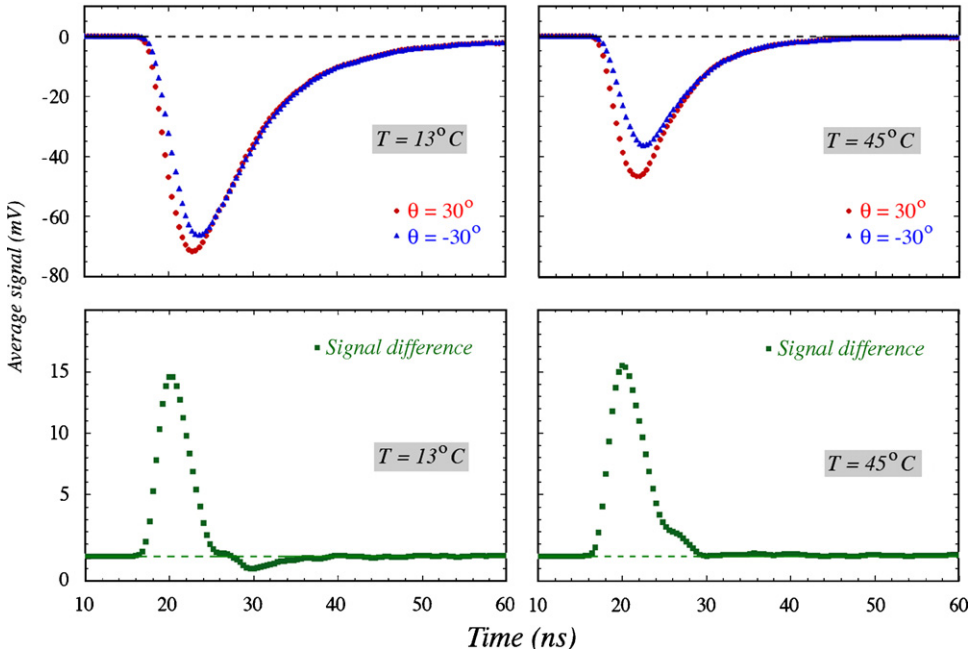

Fig. 6. Average time structure of the signals from PMT *R* measured for 50 GeV electrons traversing the $PbWO_4$ crystal at $\theta = 30^\circ$ and $\theta = -30^\circ$ (top plots), as well as the difference between these two signals (bottom plots), measured for two different temperatures: 13 °C (left) and 45 °C (right).

the showering electrons. We checked that this contamination did not change significantly during the experiments described in this paper, i.e., it was the same for all temperatures and all angles. For the analysis of these ADC data, we used the *average* signal produced by the electrons. We checked that the choice of other variables used to characterize the signal distribution (e.g., the most probable signal value, or the peak value resulting from a fit) did not change the results significantly.

2.5. Calibration of the detectors

The absolute calibration of the signals generated by the crystal was not a major concern in these tests. On the other hand, it was absolutely essential that the gains of the two PMTs, *L* and *R*, which collected the light at the two opposite ends of the crystal were equalized. We used 50 GeV electrons for that purpose. The crystal was oriented such that the beam entered the detector perpendicular to the crystal axis ($\theta = 0$), so that any Cherenkov light generated by the beam particles would be observed in the same proportion by both PMTs. The high voltages were chosen such that the average signals were about 300 ADC counts above the pedestal value (at room temperature). Off-line, the calibration constants of the ADCs (GeV/count) were fine-tuned such as to equalize the responses of the two PMTs.

For the time structure measurements, no separate calibration effort was performed. We only made sure that the vertical oscilloscope scale was chosen such that no pulse clipping occurred. As the crystals were rotated to larger angles θ, the signals increased and the scale had to be adjusted, e.g., from 100 to 200 to 500 mV full range.

3. Experimental results

3.1. Response anisotropy and time structure

All crucial aspects of the experimental results obtained in this study and discussed below are illustrated in Fig. 6. This figure shows the average time structure of the signals from one of the PMTs reading out the crystal (*R*, see Fig. 1), for the lowest and highest temperatures at which these measurements were performed: $T = 13^\circ$ (left) and $T = 45^\circ$ (right), respectively.

Each of the top graphs depicts the average time structures of the signals measured at $\theta = 30^\circ$ and $\theta = -30^\circ$. The difference between the signals recorded at these two angles is shown in the bottom graphs, separately for each of the two temperatures. At $\theta = 30^\circ$, Cherenkov light produced in the showers initiated in the crystals by the high-energy electrons is preferentially detected in PMT *R*, since this light is emitted at an angle of arccos $(1/n) = 63^\circ$ by the charged relativistic shower particles traversing the $PbWO_4$ crystal (which has a refractive index $n = 2.2$). This Cherenkov light manifests itself as an additional prompt component, superimposed on the scintillation light that constitutes practically the entire signal measured at $\theta = -30^\circ$. As a result, the signals measured at $\theta = 30^\circ$ are larger, and rise steeper than those measured with the same PMT at $\theta = -30^\circ$.[8] These effects were also observed in our previous studies, in which we established the contribution of Cherenkov light to the $PbWO_4$ signals, albeit it with a considerably inferior time resolution [1].

However, Fig. 6 also exhibits several other interesting features:

- The total, time-integrated signals are considerably smaller at the higher temperature.
- This decrease in total signal seems to be entirely due to a reduction of the amount of scintillation light, since the total Cherenkov signal is not significantly different at these two temperatures.
- As a result, Cherenkov light represents a much larger fraction of the total signal at the higher temperature.
- Less clear, but nevertheless very significant is the fact that the signal decreases much faster beyond its maximum at the higher temperature.

In the next subsections, we elaborate on all these effects.

[8] For PMT *L*, the opposite effect was observed. As expected, here the signals at $\theta = -30^\circ$ were measured to be larger and steeper than those at $\theta = 30^\circ$.

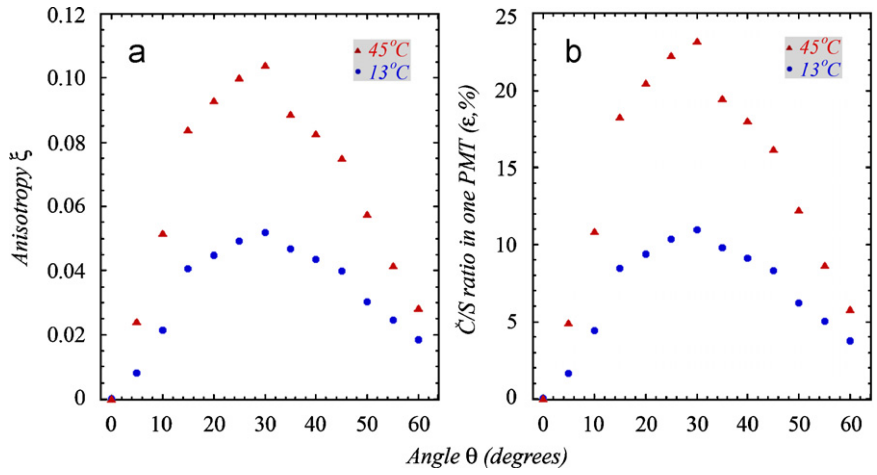

Fig. 7. The response anisotropy ξ (a) and the Cherenkov/scintillation signal ratio in PMT R, ε_R, (b) as a function of the angle of incidence (θ) of the 50 GeV e^- beam, measured at the temperatures of 13 and 45 °C. Both variables reach their maximum value near the complement of the Cherenkov angle ($90^\circ - \theta_C = 27^\circ$).

3.2. Response anisotropy and the Cherenkov fraction

We define the *response anisotropy* ($\xi \geqslant 0$) at the angle θ as

$$\xi(\theta) = \left|\frac{(R_\theta - L_\theta) + (L_{-\theta} - R_{-\theta})}{(R_\theta + L_\theta) + (L_{-\theta} + R_{-\theta})}\right| \quad (1)$$

where R_θ and L_θ represent the average signals measured in the PMTs R and L for the same events, when the crystal is oriented at an angle θ. Since these signals were equalized for $\theta = 0$, a non-zero value of ξ is indicative for a non-isotropic component in the light generated in the crystals, i.e., Cherenkov light.

The relationship between ξ and the relative contribution of Cherenkov light to the PMT signals[9] can be seen as follows. Let us call the relative contributions of Cherenkov light to the R and L signals ε_R and ε_L, respectively (with ε_R and ε_L normalized to the scintillation signals). Because of symmetry considerations, $\varepsilon_R(\theta) = \varepsilon_L(-\theta)$ and $\varepsilon_L(\theta) = \varepsilon_R(-\theta)$. Therefore,

$$\xi(\theta) = \left|\frac{\varepsilon_R(\theta) - \varepsilon_L(\theta)}{2 + \varepsilon_R(\theta) + \varepsilon_L(\theta)}\right| \quad (2)$$

The fraction of Cherenkov light in the *sum* of the two PMT signals R and L equals

$$f_C(\theta) = \frac{\varepsilon_R(\theta) + \varepsilon_L(\theta)}{2 + \varepsilon_R(\theta) + \varepsilon_L(\theta)} \quad (3)$$

Let us first consider a single relativistic charged particle traversing the $PbWO_4$ crystal. If we ignore the effects of Fresnel reflection, the acceptance of the Cherenkov light emitted by that particle is limited to one PMT only. In that case, $f_C(\theta) = \xi(\theta)$, i.e., the measured response anisotropy represents the relative contribution of Cherenkov light to total signal detected by the two PMTs combined. This fraction is zero for $\theta = 0$ and reaches its maximum possible value when Cherenkov light is emitted parallel to the crystal axis. This happens when $\theta = 90^\circ - \theta_C$, in which case the Cherenkov light is detected in PMT R, or $\theta = \theta_C - 90^\circ$ (Cherenkov light detected in PMT L). At these angles, the ratio of the contributions of Cherenkov and scintillation light to the signals from the PMT that detects the Cherenkov light also reaches its maximum value. For example, at $\theta = 90^\circ - \theta_C$

$$\varepsilon_{R,max} = \frac{2\xi_{max}}{1 - \xi_{max}} \quad (4)$$

In developing showers, the shower particles that emit Cherenkov light each travel in a different direction. In that case, both PMTs may detect a fraction of the emitted Cherenkov light, i.e., both ε_R and ε_L are non-zero. From Eqs. (2) and (3), we see that in that case

$$f_C(\theta) > \xi(\theta) \quad (5)$$

i.e., the measured response anisotropy underestimates the total Cherenkov fraction. This discrepancy increases of course as the showers further develop and the angular distribution of the shower particles that emit Cherenkov light becomes more isotropic. In calorimeters that fully contain the shower, any remaining response anisotropy reflects mainly the processes that take place in the early stages of the shower development [5].

Fig. 7 shows the measured value of the response anisotropy (a) and the Cherenkov/scintillation ratio in the signals from one PMT derived from this value (b) as a function of angle, for 50 GeV electrons traversing the $PbWO_4$ crystal. Results are given for the highest (45 °C) and the lowest (13 °C) temperatures at which complete angular scans were performed. The results obtained for the other temperatures at which such scans were done (25 and 35 °C) are consistent with those shown in Fig. 7. As expected, the anisotropy reaches its maximum value near the angle $|\theta| = 90^\circ - \theta_C$ at which Cherenkov light emitted by the incoming particles impinges perpendicularly onto the photocathode of one of the PMTs.

The response anisotropy measured at the angles $\theta = 25^\circ$, 30° and 35° is shown as a function of the temperature in Fig. 8. It increases by about a factor of two over the temperature range considered here: for example, from 4.7% at 12.3 °C to 10.4% at 45.4 °C, for $\theta = 30^\circ$. These data also show that the largest anisotropy is reached for angles $\theta = 25-30^\circ$ at all temperatures.

3.3. Time structure and the Cherenkov fraction

As illustrated in Fig. 6, the time structure of the PMT signals can also be used to determine the relative contributions of the prompt Cherenkov light. In order to get a correct measurement of the Cherenkov fraction, one needs a reference signal that does not contain a Cherenkov component. If that reference signal does contain a contribution of Cherenkov light, then the measurements will underestimate the Cherenkov fraction correspondingly.

[9] It should be emphasized that this discussion concerns the PMT signals, and *not* the number of photons produced by the different mechanisms. For the latter, differences in production spectra and photocathode quantum efficiencies would have to be taken into account.

We have chosen as reference for the signals from PMT R the time structure measured at $\theta = -30^\circ$ (see Fig. 6) and for PMT L the time structure measured at $\theta = 30^\circ$. When comparing signals measured at other angles with these reference signals, one should take into account that the effective thickness of the crystal depends on its orientation with respect to the particle beam, i.e., on the angle θ. For that reason, we normalized the trailing edge of the time structure measured at angle θ to that of the reference signal. In practice, we equalized the integrated charge measured from $t = 26-50$ ns (cf. Figs. 3 and 6), assuming that this part of the time spectra contained only contributions from scintillation light. The contribution of Cherenkov light was determined from the excess charge measured in the normalized signal with respect to the reference signal. This procedure was followed separately for both PMTs.

Fig. 9 shows the average fraction of the total signal represented by the prompt component found in this way, as a function of the angle θ. Results are given for the highest (45 °C) and the lowest (13 °C) temperatures at which measurements were performed, separately for both PMTs. The symmetry between the results for both PMTs is excellent, i.e., the results for PMT L are, within experimental uncertainties, the same as for PMT R if the sign of θ is inverted. As in the case of the response anisotropy, the largest fraction represented by the prompt signal component was found at $|\theta| \sim 90^\circ - \theta_C$. And as before, this maximum (and thus the relative fraction of Cherenkov light in the signals) increased by more than a factor of two over the temperature range considered here, from ~8% at 13 °C to ~17% at 45 °C.

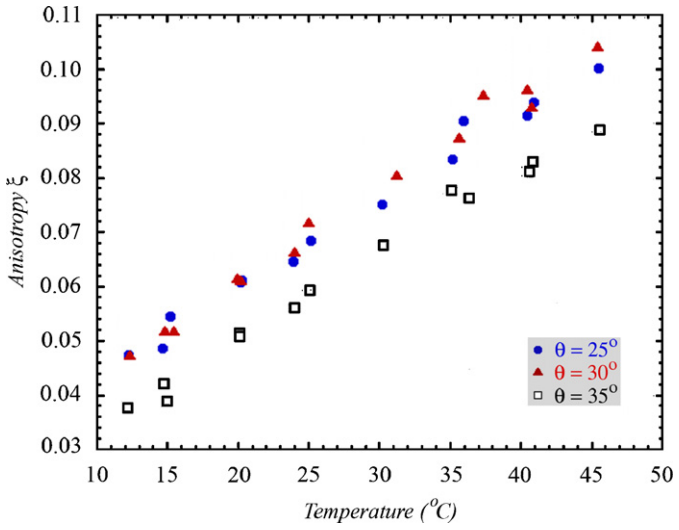

Fig. 8. The response anisotropy for 50 GeV electrons at $\theta = 25^\circ$, 30° and 35° as a function of the temperature.

However, the figure also exhibits some features that were not revealed by the measurements of the anisotropy. For example, it turns out that at $\theta = 0$, the signals from both PMTs contain a substantial Cherenkov component. The amplitude of this component is about half of that observed at the angle where the prompt component is strongest. It also appears that the signals at the "anti-Cherenkov angle", i.e., the signals that were used for "pure" scintillation reference purposes, were not so pure after all. In fact, the prompt component seems to reach a local, secondary maximum precisely at that angle.

One factor contributing to this phenomenon is Fresnel reflection. For light impinging perpendicularly at the interface between two media with indices n_{in} and n_{out}, the reflection coefficient f_R is equal to

$$f_R = \left[\frac{n_{in} - n_{out}}{n_{in} + n_{out}}\right]^2 \quad (6)$$

This gives a probability of ~5% that Cherenkov light reflects at the interface between the crystal ($n_{in} = 2.2$) and the cookies ($n_{out} = 1.403$) and is detected by the PMT at the opposite end of the crystal. However, the size of the effects observed in Fig. 9 suggests that Fresnel reflection is not the only factor responsible for it. Other contributions may come from the optical properties of the crystal surfaces, such as the quality of the polishing and the wrapping material. More studies are needed to understand these effects in sufficient detail.

In any case, by choosing the time structure of the signals at the "anti-Cherenkov angle" as the (promptless) scintillation reference, the contribution of the prompt component, and thus of Cherenkov light, to the PMT signals is systematically underestimated.

3.4. Temperature dependence of the Cherenkov fraction

The analyses described in the previous subsections were repeated for all other temperatures at which measurements were performed. For all temperatures, data were collected at $\theta = 0$, which made it possible to intercalibrate the two PMT signals, and at $\theta = \pm 25^\circ, \pm 30^\circ$ and $\pm 35^\circ$, i.e., the region in which the maximum response anisotropies and prompt signal fractions were measured to occur (see Figs. 8 and 9). This makes it possible

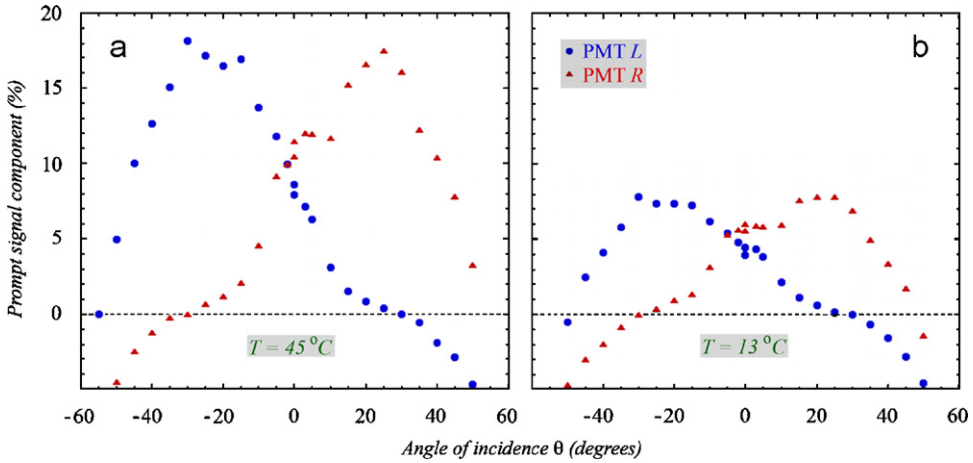

Fig. 9. Fraction of the total signal represented by the prompt component, as a function of the angle of incidence (θ) of the 50 GeV e^- beam, measured at temperatures of 45 °C (a) and 13 °C (b). Results are shown separately for PMT L (where the fraction is normalized to zero for $\theta = 30^\circ$) and PMT R (normalized to zero for $\theta = -30^\circ$).

to study the fraction of Cherenkov light as a function of the temperature.

The results are shown in Fig. 10, which gives the ratio of the Cherenkov and scintillation contributions to the signals from a single PMT, derived from the response anisotropy ξ and from the time structure of the signals, at the angle for which this ratio reaches its maximum value ($|\theta| = 30^\circ$), as a function of the temperature of the crystal. The time structure data were averaged over both PMTs for this purpose.

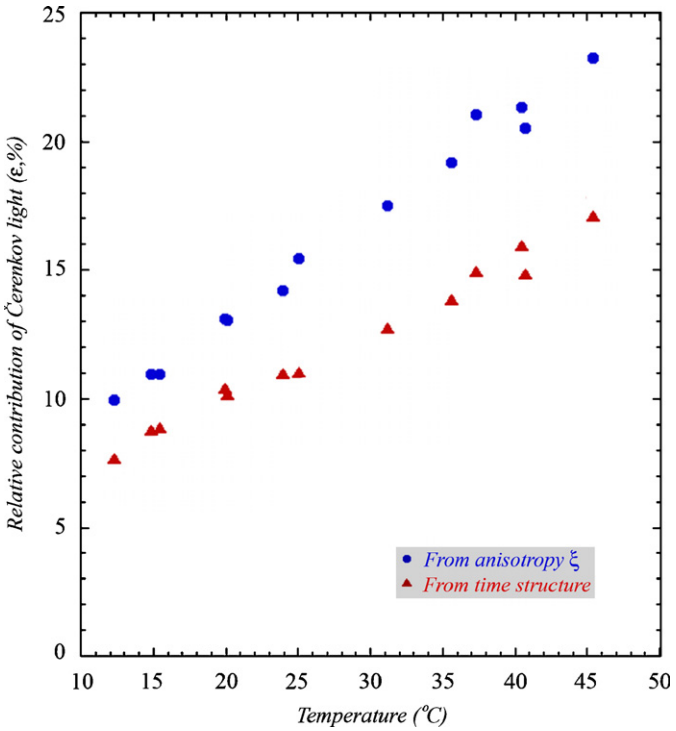

Fig. 10. Temperature dependence of the Cherenkov/scintillation signal ratio, ε, measured in one of the PMTs reading out the $PbWO_4$ crystal. This ratio is derived from the response anisotropy, or from the relative contribution of the prompt component to the signals (averaged over the two PMTs). Data for 50 GeV electrons traversing the crystal at the angle for which Cherenkov light impinges (approximately) perpendicularly onto the PMT: $\theta = 30^\circ$ for PMT *R*, -30° for PMT *L*.

Apart from the fact that the measurement of this C/S ratio from the time structure data leads to a systematically underestimated value (see Section 3.3), the results from these two methods are in good agreement with each other. Both methods indicate a substantial and gradual increase in the fraction of Cherenkov light, as the temperature increases. Over a temperature range of 32 °C, the Cherenkov/scintillation ratio was measured to more than double in value, from ≈ 0.10 at 13 °C to ≈ 0.23 at 45 °C.

3.5. Temperature dependence of the light yield

The gradual and substantial increase in the fraction of Cherenkov light in the signals from the $PbWO_4$ crystal that is observed as the temperature rises (Fig. 10) is the result of a *decrease* in the amount of scintillation light produced by the crystal. This may already be concluded from Fig. 6, which shows that the prompt component is the same for both temperatures, but that the overall signal is considerably smaller at the higher temperature, causing the prompt component to be much more pronounced in that case.

This conclusion was confirmed by a study of the temperature dependence of the light yield of the individual PMTs for different orientations of the crystal. Results of this study are displayed in Fig. 11. Fig. 11a shows the average signals measured in PMT *L* for $\theta = -30^\circ$, 0° and 30° as a function of the temperature, over the range from 13° to 45°. The same is shown for PMT *R* in Fig. 11b. The fact that the light yield at $\theta = \pm 30^\circ$ is larger than at 0° is a consequence of the increased (apparent) thickness of the rotated crystal; the difference observed between the light yields measured at $\theta = \pm 30^\circ$ is the result of different contributions of Cherenkov light to the signals. The results indicate in all cases an exponential decrease in the light yield as a function of temperature, since the data are reasonably well described by straight lines in these logarithmic plots. However, the slope of the fitted exponential clearly depends on the angle. The temperature dependence of the light yield, expressed in terms of this coefficient, is summarized in Table 1.

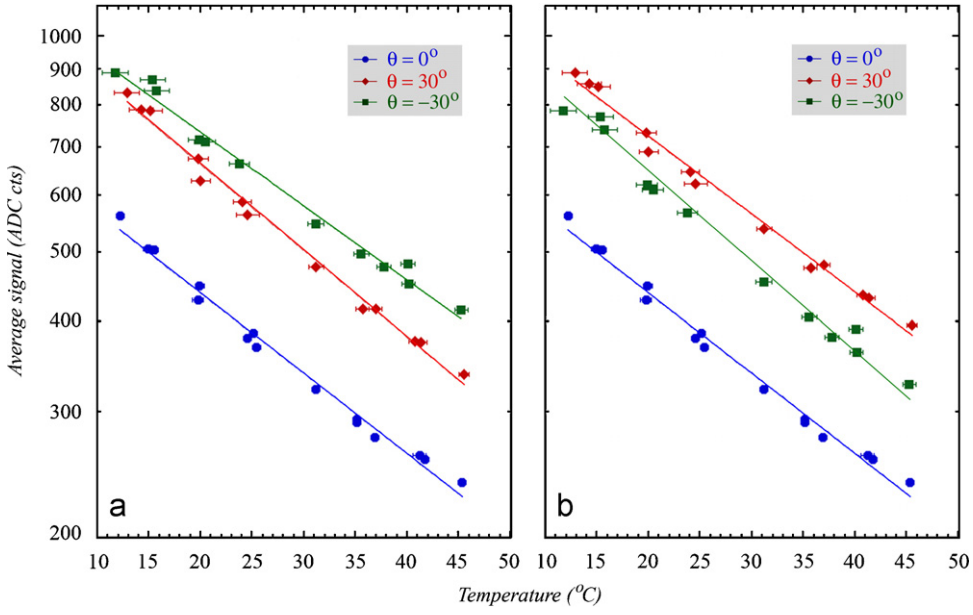

Fig. 11. Signals from the $PbWO_4$ crystal as a function of the temperature, measured with PMT *L* (a) and PMT *R* (b), for 50 GeV electrons traversing the crystal at angles $\theta = 30^\circ$, 0° and -30°. The lines represent the results of least-squares exponential fits to the experimental data. The error bars represent only statistical uncertainties.

Table 1
Temperature dependence of the light yield measured in the two PMTs reading out the $PbWO_4$ crystal, for three different orientations

Angle θ	Slope PMT L (%/°C)	Slope PMT R (%/°C)
-30°	2.61 ± 0.02	2.99 ± 0.02
0°	2.81 ± 0.02	2.80 ± 0.02
30°	2.95 ± 0.02	2.66 ± 0.02

Errors are statistical only.

It turns out that the decrease in the light yield for increasing temperatures is considerably steeper when the signals contain no (or very little) Cherenkov light, i.e., at $\theta = -30^\circ$ for PMT R and at $\theta = 30^\circ$ for PMT L. In those cases, the light yield decreases by 2.97%/°C, compared with 2.64%/°C for angles at which the Cherenkov content of the signals is largest. For $\theta = 0$, a value of 2.80%/°C was measured, indicating that there was at least some Cherenkov light contributing to the signals. It is noteworthy that this angular dependent pattern of the temperature coefficients is perfectly consistent for the two PMTs, i.e., the measured slopes for $\theta(R)$ and $-\theta(L)$ are the same within experimental errors.

Similar results as shown in Fig. 11 and Table 1 were obtained by using instead of the ADC data the integrated time structure profiles of the signals (shown, for example, in Fig. 6). A combined analysis of the light yield (Fig. 11) and the fraction of Cherenkov light in the total signal (Fig. 10) as a function of temperature thus confirmed the fact, already observed in Fig. 6, that the intensity of the Cherenkov light generated by the 50 GeV electrons in the $PbWO_4$ crystals is indeed *independent* of the temperature. All temperature dependent effects observed in this crystal concern *only* the scintillation process. Combining all data, we conclude that the scintillation light yield decreases at a rate of 2.97 ± 0.04%/°C. Depending on the angle of incidence, and thus on the relative contribution of (temperature independent) Cherenkov light to the signals, this rate may decrease to as much as 2.64 ± 0.05%/°C. These results may be compared with the rate of 2.7 ± 0.1%/°C reported by Zhu in the Particle Data Review [6].

3.6. Temperature dependence of the decay constant

When the time structure of the PMT signals is displayed logarithmically, yet another temperature dependent effect of the scintillation process becomes visible.

Fig. 12 shows the time structure of the (inverted) signals measured with PMT L at $\theta = 30^\circ$, for the highest (45 °C) and the lowest (13 °C) temperatures at which measurements were performed. The trailing edge of the signal is considerably steeper at the higher temperature. This trailing edge is reasonably well described by a single exponential. The straight lines drawn in this figure correspond to a decay time of 5.6 ns at 45° vs. 8.8 ns at 13 °C. We want to re-emphasize that these results concern one particular crystal, and that the decay time of other, similar crystals is not necessarily the same. For example, we measured previously a decay time of 9.7 ns at room temperature for a crystal from the same source [5], and other authors have reported decay times around 10 ns as well [7]. Yet, the temperature dependence of the decay time is a feature we have also observed for other $PbWO_4$ crystals.

We have studied the temperature dependence of the decay time of this particular crystal in a systematic way at all the different temperatures at which measurements were performed. Since the decay concerns the scintillation process, we concentrated on signals in which the Cherenkov contribution was minimal, i.e., the signals from PMT L at $\theta = 30^\circ$ and the $\theta = -30^\circ$ signals from PMT R. The trailing edge of the average time structure profile was fit to an exponential function over a range starting 2 ns after the maximum amplitude was reached and extending to the point where the signal had dropped to 13.5% (e^{-2}) of the amplitude value. The results are summarized in Table 2 and graphically displayed in Fig. 13.

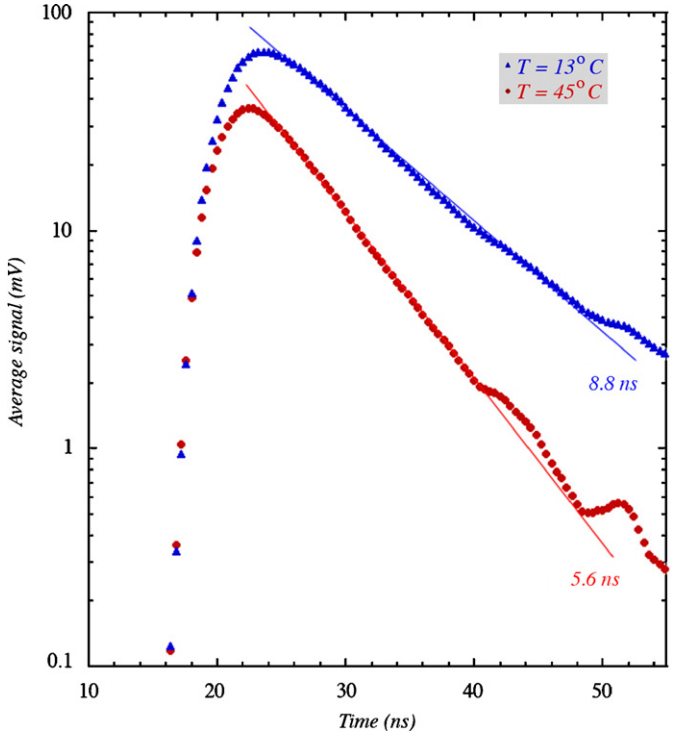

Fig. 12. Average time structure of the $PbWO_4$ signals from PMT L for $\theta = 30^\circ$, measured at two different temperatures. The straight lines are drawn to guide the eye.

Table 2
Decay time of the scintillation signals from the $PbWO_4$ crystal for different temperatures

Temperature (°C)	Decay time (ns) PMT L, $\theta = 30^\circ$	Decay time (ns) PMT R, $\theta = -30^\circ$
13	7.97 ± 0.11	9.35 ± 0.13
15	7.70 ± 0.11	8.86 ± 0.12
20	7.07 ± 0.11	8.04 ± 0.12
25	6.73 ± 0.11	7.48 ± 0.12
30	6.27 ± 0.11	6.68 ± 0.12
35	5.96 ± 0.11	6.25 ± 0.12
40	5.76 ± 0.11	6.05 ± 0.12
45	5.70 ± 0.11	5.78 ± 0.14

The errors include only statistical uncertainties.

These data show that the decay time of the scintillation light produced in $PbWO_4$ crystal gradually decreases by 30–40% over the temperature range from 13 to 45 °C. This effect is observed in both PMTs. The decay times measured with PMT R are systematically somewhat larger than those measured with PMT L. It is unclear which systematic effect is responsible for this difference.

A gradual decrease in the decay time of the luminescence was also reported by Millers and coworkers [3], who studied the properties of $PbWO_4$ in the temperature range from 100 to 300 K with a high-intensity pulsed beam of low-energy electrons. The temperature dependence of this effect turned out to be quite different for different temperature regions, and the authors concluded from this that the mechanism responsible for it is very

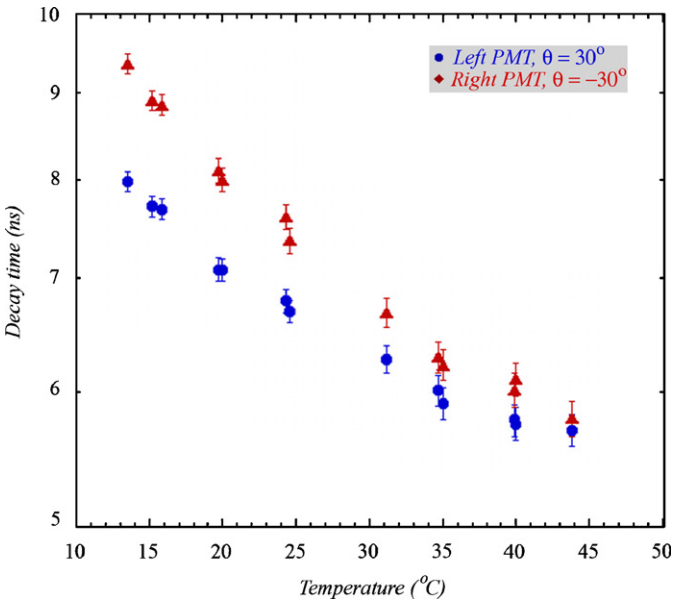

Fig. 13. The decay constant of the scintillation light produced by the $PbWO_4$ crystal, as a function of temperature. Data for 50 GeV electrons traversing the crystal at an angle at which the signals are almost exclusively generated by scintillation light, i.e., 30° for PMT *L* or −30° for PMT *R*. The error bars represent only statistical uncertainties.

different in the cryogenic region (100–170 K) than at higher temperatures. Since the authors concentrated on the long-lived components of the luminescence, a further detailed comparison with our results is not very meaningful.

4. Conclusions

When a complex crystalline compound such as lead tungstate is brought into an excited state, it can fall back to the ground state through several mechanisms. Emission of scintillation light in the visible region of the optical spectrum as a result of electronic transitions is one such mechanism. However, non-radiative processes and processes in which radiation in the non-visible domain is emitted also play a role. As the temperature increases, both the number of competing processes through which the excited crystal may relax, as well as the efficiency of such processes increase. As a result, the decay width increases, the lifetime of the excited state decreases, and the probability that the crystal de-excites by emitting visible scintillation light decreases as well.

All phenomena observed in our study are consistent with such a scenario, known as thermal quenching of the luminescence [3]. As the temperature of the $PbWO_4$ is increased, the light yield decreases considerably, and the decay time of the pulses decreases as well. Since these effects only concern the scintillation component of the light generated by the showering electrons, and not the Cherenkov light also produced in this process, the Cherenkov fraction of the signals increases correspondingly as the temperature of the crystals is increased. This increased Cherenkov fraction is an interesting feature for application of these crystals in dual-readout calorimeters.

Acknowledgments

We thank CERN for making particle beams of excellent quality available for the study described in this paper. This study was carried out with financial support of the United States Department of Energy, under contract DE-FG02-07ER41495.

References

[1] N. Akchurin, et al., Nucl. Instr. and Meth. A 582 (2007) 474.
[2] P. Lecoq, Nucl. Instr. and Meth. A 537 (2005) 15.
[3] D. Millers, et al., Phys. Status Solidi (b) 203 (1997) 585.
[4] R. Mao, L. Zhang, R. Zhu, Nucl. Instr. and Meth. A 537 (2005) 406.
[5] N. Akchurin, et al., Nucl. Instr. and Meth. A 584 (2007) 273.
[6] W.-M. Yao et al. (Particle Data Group), J. Phys. G 33 (2006) 1 (Table 28.4).
[7] P. Lecoq, A. Annenkov, A. Gektin, M.B. Korzhik, C. Pedrini, Inorganic Scintillators for Detector Systems: Physical Principles and Crystal Engineering, Springer, Berlin, 2006 (and references therein).